ACES Asian Chemical Editorial Society
DOI: 10.1002/asia.201900030
CHEMISTRY AN ASIAN JOURNAL Minireview

Biomass-Derived Carbon Materials as Prospective Electrodes for High-Energy Lithium- and Sodium-Ion Capacitors

Subramanian Natarajan,[a] Yun-Sung Lee,*[b] and Vanchiappan Aravindan*[a]

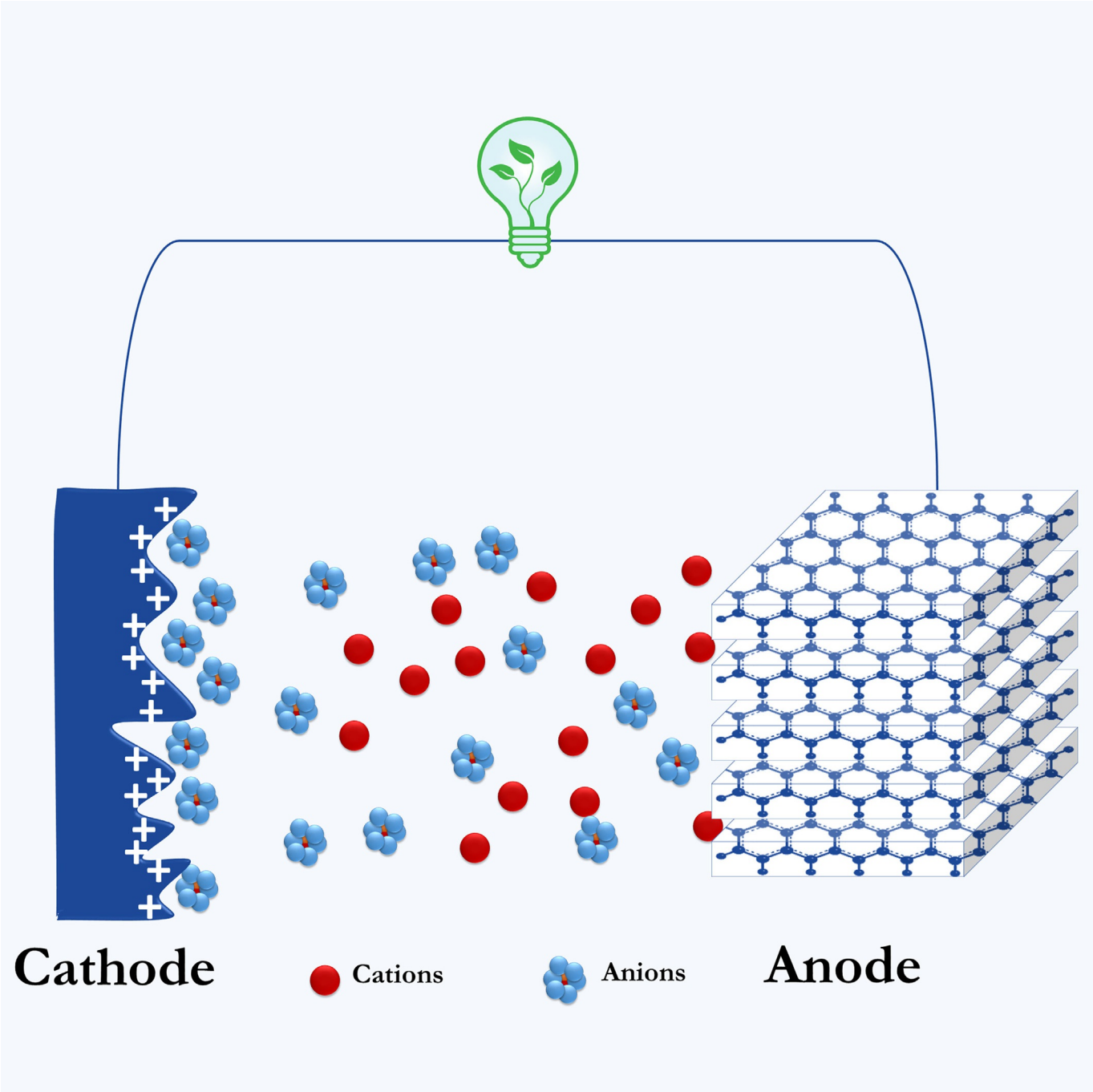

Abstract: Biomass-derived carbon materials have received special attention as efficient, low-cost, active materials for charge-storage devices, regardless of the power system, such as supercapacitors and rechargeable batteries. In this Minireview, we discuss the influence of biomass-derived carbonaceous materials as positive or negative electrodes (or both) in high-energy hybrid lithium-ion configurations with an organic electrolyte. In such hybrid configurations, the electrochemical activity is completely different to conventional electrical double-layer capacitors; that is, one of the electrodes undergoes a Faradaic reaction, whilst the counter electrode undergoes a non-Faradaic reaction, to achieve high energy density. The use of a variety of biomass precursors with different properties, such as surface functionality, the presence of inherent heteroatoms, tailored meso-/microporosity, high specific surface area, various degrees of crystallization, calcination temperature, and atmosphere, are described in detail. Sodium-ion capacitors are also discussed, because they are an important alternative to lithium-ion capacitors, owing to the low abundance and high cost of lithium. The electrochemical performance of carbonaceous electrodes in supercapacitors and rechargeable batteries are not discussed.

1. Introduction

Supercapacitors, often called "ultra-capacitors", have gained special attention in recent years, owing to their high power capability, long lifecycle, high round-trip efficiency, and low cost.[1] However, their limited energy density is the main obstacle to their implementation when high energy demand is required. Typically, electrical double-layer capacitors (EDLCs), often called supercapacitors, are fabricated from high-surface-area carbonaceous materials in the presence of aqueous solution. To date, a variety of carbonaceous materials, that is, allotropes such as graphene, porous carbon materials, carbon nanotubes (single, double, and multi-walled), and aerogels, have been explored as supercapacitors, but activated carbon (AC) remains the most-popular choice for prospective electrodes.[2–5] In a typical configuration, high-surface-area carbonaceous materials form a double layer across an electrode/electrolyte interface through the accumulation of charge carriers over the surface. Such physical adsorption/desorption, that is, double-layer formation, certainly translates high power capability to the system.[3,5,6] However, disappointingly, the decomposition potential of water (ca. 1.23 V) hampers the high energy density of conventional EDLCs.

To increase the energy density of such aqueous-solution-based supercapacitors, organic solutions (including ionic liquids) have been introduced and have exhibited electrochemical stabilities of up to 3.5 V. Although the working potential is extended in such cases, the energy density is still far behind the reality, owing to inferior ionic mobility and high viscosity. In such cases, the solvent that is used to dissolve the charge carrier cannot be simply ignored, and it plays a vital role in determining energy density, thereby diluting the high power capability of the system compared to aqueous-based assemblies. In addition, the discovery of fast Faradaic reactions, that is, pseudocapacitance on the surface of nanostructured transition metal oxides (later extended to sulfides) has led to opportunities to construct asymmetric supercapacitors (ASCs) with aqueous-based solutions at wider potentials.[7–10] Similar to AC, the Faradaic reaction is related to the specific surface area of the transition metal oxide. Typically, a transition metal oxide that undergoes a Faradaic reaction is engaged as a positive terminal and AC remains as a negative electrode for a wide range of alkali metal ions (Na^+, Li^+, K^+, etc.). MnO_2 is a perfect example of a positive electrode for use in ASCs, regardless of structural properties,[9,11,12] which leads to a notable increase in energy density compared to symmetrical assemblies, as in EDLCs. Similar kinds of studies have also been conducted in organic-based solutions, in which the pseudocapacitance component is replaced with (mostly) insertion-type electrodes (a perfect Faradaic reaction in which the bulk is involved in the reaction, rather than the surface; in some cases, conversion and alloying have been employed) and the AC acts as a counter electrode in the presence of a Li^+-containing organic solution. This new configuration has been termed "lithium-ion capacitors" (LICs), or lithium-ion hybrid electrochemical capacitors; for example, insertion-type spinel $Li_4Ti_5O_{12}$ has been used as a negative electrode, with AC as a positive electrode. Typically, this configuration offers the combined advantages of EDLCs and lithium-ion batteries, that is, the high power capability of lithium-ion batteries and the high energy density of conventional EDLCs.[13–15] Numerous lithium-insertion-type materials have been proposed as negative electrodes for LICs, along with AC as a counter electrode, such as anatase and bronze phases of TiO_2, TiS_2, $TiSe_{0.6}S_{1.4}$, TiP_2O_7, $TiNb_2O_7$, FeOOH, MnO_2, $LiCrTiO_4$, $LiTi_2(PO_4)_3$, $LiNi_{0.5}Mn_{1.5}O_4$, and $Li_3V_2(PO_4)_3$, which includes graphite and hard carbon.[13,16–19] Similar to anodes, lithium-ion battery cathodes have also been explored for LIC applications, such as $LiMn_2O_4$, $LiNi_{0.5}Mn_{1.5}O_4$, $Li_3V_2(PO_4)_3$, and $LiFePO_4$, in which AC has been used as a negative electrode.[13,14,20] Owing

[a] *Dr. S. Natarajan, Dr. V. Aravindan*
Department of Chemistry
Indian Institute of Science Education and Research (IISER)
Tirupati 517507 (India)
E-mail: aravind.van@gmail.com

[b] *Prof. Y.-S. Lee*
Faculty of Applied Chemical Engineering
Chonnam National University
Gwang-ju 500-757 (Republic of Korea)
E-mail: leeys@chonnam.ac.kr

Supporting information and the ORCID identification number(s) for the author(s) of this article can be found under:
https://doi.org/10.1002/asia.201900030.

to its fascinating features, specifically wider electrochemical stability, AC can be used as either a negative or positive electrode.[3] We have previously reported a detailed exploration of various insertion-type materials for LICs.[13] Although high energy density is possible with a Faradaic-type electrode, realizing high power capability remains an issue, owing to the limited lithium-ion-diffusion kinetics. Nevertheless, owing to extensive research activities, carbon coating and composites with carbonaceous counterparts have been realized as effective solutions for improving the power capability/high rate performance of the electrodes, as extensively described in our previous review.[13,20] Notably, modification of the battery-type electrode with carbonaceous materials leads to dilution of the volumetric energy density.[21,22] Alternatively, by tuning the properties of the counter electrode, such as specific surface area, surface functionalization, porosity, and heteroatom doping, the power density of the system can be increased, without compromising the volumetric energy density. Such modifications in carbonaceous electrodes have been extensively studied from an EDLC point of view, but limited research has been performed from a LIC perspective. Furthermore, most of the LIC work has dealt with the performance of commercially available AC, but no in-depth studies have been performed, because one electrode undergoes a Faradaic process, whereas another electrode obeys a non-Faradaic charge-storage process.[23–28] The use of biomass-derived carbon offers several advantages, such as active surface functional groups (hydroxy and carboxy) and naturally abundant heteroatom doping (N, S, etc.), which results in an increase in specific capacitance and, eventually, enhanced energy and power densities.[29,30] Furthermore, the electrical conductivity is also increased and the porosity (mesoporosity/microporosity ratio) can be tailored according to the requirements with a very high specific surface area.

The utilization of biomass waste in the production of electrode materials is a smart way of cutting the costs of the raw materials without compromising the positive environmental impact. To date, a large number of biomass-derived carbon materials have been extensively reported in both symmetric and asymmetric configurations, with improved electrochemical properties[31] compared to commercially available AC.[32–38] However, disappointingly, there has been very limited work on their use in LIC assemblies. As such, this Minireview describes the performance of such biomass-derived carbonaceous materials in LIC configurations. Currently, sodium-ion chemistry is booming as a low-cost energy-storage technology, and it is thought to be a strong contender for replacing lithium-ion-based systems in the near future.[19,20,39,40] However, sodium-intercalation materials are highly limited, unlike those with lithium-insertion hosts, mainly because of the increased Coloumbic Na–Na interactions, which make exploring the appropriate insertion host with high reversibility much more complex.[41] Still, there have been a few reports on the efficient utilization of biomass-derived carbon for sustained sodium storage in sodium-ion capacitors (NICs).[20] Therefore, the electrochemical activity of such biomass-derived carbonaceous materials in both lithium-ion and sodium-ion capacitor assemblies is interesting for further exploration, and is also extensively described in this Minireview.

2. Rice Husk

Rice husk (RH) is an important type of biomass from the agricultural sector and, of course, the milling industry. The conversion of RH into useful charge-storage materials would be very effective, because RH is composed of a variety of metal oxides (K_2O, Na_2O, MgO, CaO, Fe_2O_3, and silica).[42] Furthermore, the presence of a cellulose derivative leads to a carbon content of 37%. Several attempts have been made to explore this material as an anode in lithium-ion batteries.[43] Babu et al. studied the possibility of using RH-derived activated carbon (RH-AC) as an EDLC component in LIC configurations with insertion-type $Li_4Ti_5O_{12}$.[44] The authors used two different activating agents (H_3PO_4 and KOH) for hydrochar, which afforded surface areas

Subramanian Natarajan is a Postdoctoral Research Fellow in the laboratory of Dr. V. Aravindan at the Indian Institute of Science Education and Research (IISER), Tirupati, India. Previously, he worked at the CSIR-Central Salt and Marine Chemicals Research Institute (CSIR-CSMCRI) with Professor Hari C. Bajaj and earned his Ph.D. in Chemistry from Maharaja Krishnakumarsinhji Bhavnagar University, Bhavnagar, India, in 2018. His research interests mainly focus on the recycling of spent lithium-ion batteries, electrochemical energy storage, and conversion technologies.

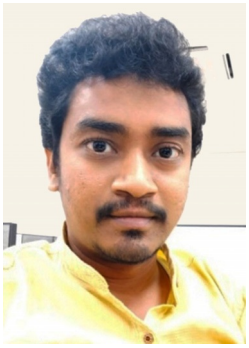

Yun-Sung Lee is a Full Professor at Chonnam National University, Gwang-ju, Republic of Korea. He received his M.Sc. from Chonbuk National University in 1998 under the guidance of Professor Kee-Suk Nahm. He received his Ph.D. in Applied Chemistry from Saga University, Japan, in 2001, under the direction of Professor Masaki Yoshio. Then, he took up a position as a Postdoctoral Fellow with Professor Yuichi Sato at Kanagawa University, Japan. In 2003, he joined Chonnam National University as an Assistant Professor. His research interests are in lithium-ion batteries, electrode materials, and hybrid capacitor systems.

Vanchiappan Aravindan is an Assistant Professor at the Department of Chemistry, Indian Institute of Science Education and Research (IISER), Tirupati, India. He received his Ph.D. from Gandhigram Rural University, Gandhigram, India, in 2009. Then, he joined Chonnam National University, Gwang-ju, Republic of Korea, as a Postdoctoral Fellow working with Professor Yun-Sung Lee. Later (2010–2017), he took up a position as a Senior Scientist at the Energy Research Institute @NTU (ERI@N), Nanyang Technological University, Singapore. His research interests include the development of high-performance electrodes and electrolytes for lithium-ion chemistry.

of about 1754 and 2303 $m^2 g^{-1}$, respectively. The purpose of using activating agents was to eradicate the presence of impurities, such as acids, alcohols, and aldehydes, in the carbon pores, thereby increasing the diameter of the pores and the surface area of the carbon materials. Both H_3PO_4 and KOH produced samples with a porous nature and a sheet-like morphology, as confirmed by TEM analysis. However, the pore volume was larger for the KOH-activated sample than for the H_3PO_4-activated sample, because it offered the astonishing effect of generating micropores. This larger pore volume and higher specific surface area resulted in unprecedented performance in the single-electrode configuration and displayed a capacity of about 58 mAh g^{-1}, compared to about 40 mAh g^{-1} for the H_3PO_4-activated process. Furthermore, a similar trend was also observed in the LIC configuration; for example, maximum energy densities of about 37 and 57 Wh kg^{-1} were reported, with significant power densities of about 7.2 and 9.7 kW kg^{-1} for the H_3PO_4- and KOH-based activation processes, respectively. This respectable electrochemical performance was mostly ascribed to the defective nature of the resultant porous carbon materials, which was instigated by the activation process. Although distinct differences between the energy and power densities were noted depending on the activation method, the cells displayed more or less the same cycling behavior.

3. Vegetable Oil

Aravindan et al. reported a synthesis of long-range-ordered, high-quality graphitic carbon materials with hollow fiber and spherical morphologies from cooking vegetable oil.[45,46] By adjusting the external temperature, they induced a change in the morphological features, regardless of the long-range-ordering process. A stainless steel plate was used as a catalyst for chemical vapor deposition at 900 °C. This external chamber temperature certainly influenced the morphological features, but not the graphitization process. Except for the stronger irreversibility in the first cycle, the reversibility, stability, and properties were in good agreement with commercial graphite powder.[47–50] The battery-type electrode material had to be pre-lithiated prior to the fabrication of the LIC with AC. In such a case, regardless of the reversibility in the first cycle, this graphitic carbon (spherical and fiber-shaped morphologies) could act as an efficient insertion host for accommodating lithium ions in an irreversible manner. Under the optimized mass loadings, the LIC delivered maximum energy densities of about 108 Wh kg^{-1} (at 0.315 kW kg^{-1}) and 112 Wh kg^{-1} (at 0.315 kW kg^{-1}) for the spherical and hollow fiber morphologies, respectively. Furthermore, very good cycling profiles were recorded for both graphitic phases at high current resting.

4. Sisal Fiber

A synthesis of graphitic carbon fibers from sisal fiber (SF) was reported by Yang et al.[51] During the synthesis process, $Ni(NO_3)_2 \cdot 6H_2O$ was used as a catalyst at high temperatures. Prior to calcination at high temperatures, a pre-calcination step was performed at 400 °C to decompose the organic groups that were present in the biomass precursor. After the calcination process, residual nickel species were removed by dipping the product in 1 M HCl solution. As expected, increasing the calcination temperature (900→1100 °C) resulted in a smaller specific surface area. Conversely, carbonization of the graphitic phase increased with temperature, as evident from XRD analysis. Furthermore, an increase in the I_D/I_G ratio from 0.85:1 to 0.94:1 on increasing the carbonization temperature ratified the influence of temperature on the development of the graphitic structure. At 1100 °C, the graphitic carbon material displayed an interlayer spacing of 0.337 nm, which was slightly wider than that of graphite, as a consequence of the blend of graphitic and turbostratic stacking interactions. Lithium-storage studies in a half-cell assembly clearly indicated that the phase formation strongly resembled a hard carbon (HC) structure, rather than graphite, as shown by the absence of characteristic features. Mesocarbon microbeads (MCMB) were also tested for comparison; however, the fibers delivered marginally better reversible capacity (ca. 361 mAh g^{-1}) than MCMB (ca. 339 mAh g^{-1}) in a half-cell configuration. Nevertheless, HC also acted as a good insertion host for LICs. The pre-lithiated phase was used as a battery-type material, along with an SF-derived AC for the construction of LICs with an active material loading of 1:1.2. The LIC delivered a maximum energy density of about 104 Wh kg^{-1} at a power density of 0.143 kW kg^{-1}, with good cycling profile (3000 cycles) and retention capability (>94%). The same group also attempted to use SF as a source for preparing AC (SF-AC).[52] As usual, a hydrothermal activation process and subsequent chemical activation with KOH at different ratios (0–3:1) were reported. Of these ratios, SF-AC (2:1) exhibited a good hierarchical porous structure that comprised macropores (diameter: ca. 1 μm), mesopores (ca. 10–20 nm), and micropores (ca. 0.6–2 nm), as examined by using pore-size distribution. Increasing the concentration of the activating agent led to increased specific surface area and pore volume. Furthermore, the same behavior was observed in the capacitance measurements in a half-cell configuration. Subsequently, a LIC was also fabricated with pre-lithiated MCMB. Upon pre-lithiation, full discharge was deliberately avoided by considering lithium plating during high-current operation. Interestingly, a higher KOH ratio (3:1) delivered a higher energy density (ca. 96 Wh kg^{-1}) at lower rates, but failed to translate such performance at higher rates (ca. 12 Wh kg^{-1}). On the other hand, a moderate KOH ratio (2:1) afforded energy densities of about 83 (at 0.13 kW kg^{-1}) and 41 Wh kg^{-1} (at 5.72 kW kg^{-1}) at lower and higher rates, respectively. Similar behavior was also reflected in the cycling profiles: very poor profiles were noted at higher concentrations, whereas a moderated ratio afforded a very stable cycling profile. This result clearly suggested that the optimization of KOH was crucial for the activation process, but that this concentration may vary on a case-by-case basis.

5. Coconut Shell

Jain and co-workers extensively studied the utilization of coconut (*Cocos nucifera*)-shell-derived AC by adopting various strategies to improve their textural properties, such as high specific

surface area, mesoporosity, oxygenated functional groups, and pore-size distribution.[53–59] Coconut shell (CS) is an important type of biowaste, owing to its low ash content (ca. 2%) and high carbonaceous content (>72%).[32,60] Physical and chemical activation (P) were performed by using $ZnCl_2$ and CO_2, respectively, to formulate CS-P from CS. Then, CS-HTP, CS-ZP, and CS-ZHTP were synthesized by using different activation conditions, followed by hydrothermal treatment (HT). This technique maximized the mesoporosity by creating more oxygen functional groups in the carbon materials. The microporous nature of CS-P and CS-HTP was confirmed from their type-I isotherms, whereas CS-ZP and CS-ZHTP exhibited type-II and type-IV isotherms, respectively. The BET surface areas of CS-P, CS-ZP, CS-HTP, and CS-ZHTP were 533(±29), 1421(±75), 712(±2), and 1652(±132) $m^2 g^{-1}$, respectively. The performance of these materials in single electrodes (half-cells) was evaluated to ascertain the best candidate for pairing with a battery-type $Li_4Ti_5O_{12}$ anode between 3–4.6 V (vs. Li) and also to balance the mass loading between the electrodes. This potential window allowed the anions in the electrolyte solution (PF_6^-) to be involved in the double-layer formation with their carbonaceous counterpart.[61] Accordingly, specific capacitances of about 11, 99, 132, and 159 $F g^{-1}$ were obtained for CS-P, CS-HTP, CS-ZP, and CS-ZHTP, respectively (Figure 1). The order of the specific capacitance was consistent with the order of the corresponding specific surface area, that is, 533, 712, 1421, and 1652 $m^2 g^{-1}$ for CS-P, CS-HTP, CS-ZP, and CS-ZHTP, respectively. Furthermore, the high capacitance of CS-ZHTP was attributed to the availability of a higher percentage of mesopores (ca. 60%) than in CS-ZP (ca. 48%), and CS-ZHTP (ca. 20%), which boosted the electrochemical performance. Consequently, a LIC was fabricated by tuning the loading of the coconut-shell-derived AC with respect to the $Li_4Ti_5O_{12}$ anode. As expected, CS-ZHTP delivered a maximum energy density of about 69 Wh kg^{-1}, followed by about 52 and 36 Wh kg^{-1} at a power of 0.5 kW kg^{-1} for CS-ZP and CS-HTP, respectively. Nevertheless, all three materials displayed good cycling behavior, with about 85% retention after 2000 cycles. Furthermore, the same group also explored the possibility of using CS-ZP as a counter electrode with high-capacity, electrospun $TiNb_2O_7$ as a battery-type component instead of $Li_4Ti_5O_{12}$.[62] Disappointingly, CS-ZP/$TiNb_2O_7$ functioned over a wide potential range (0–3 V) and, hence, the energy density would be eventually diluted. Nevertheless, high energy density (ca. 43 Wh kg^{-1}) and power densi-

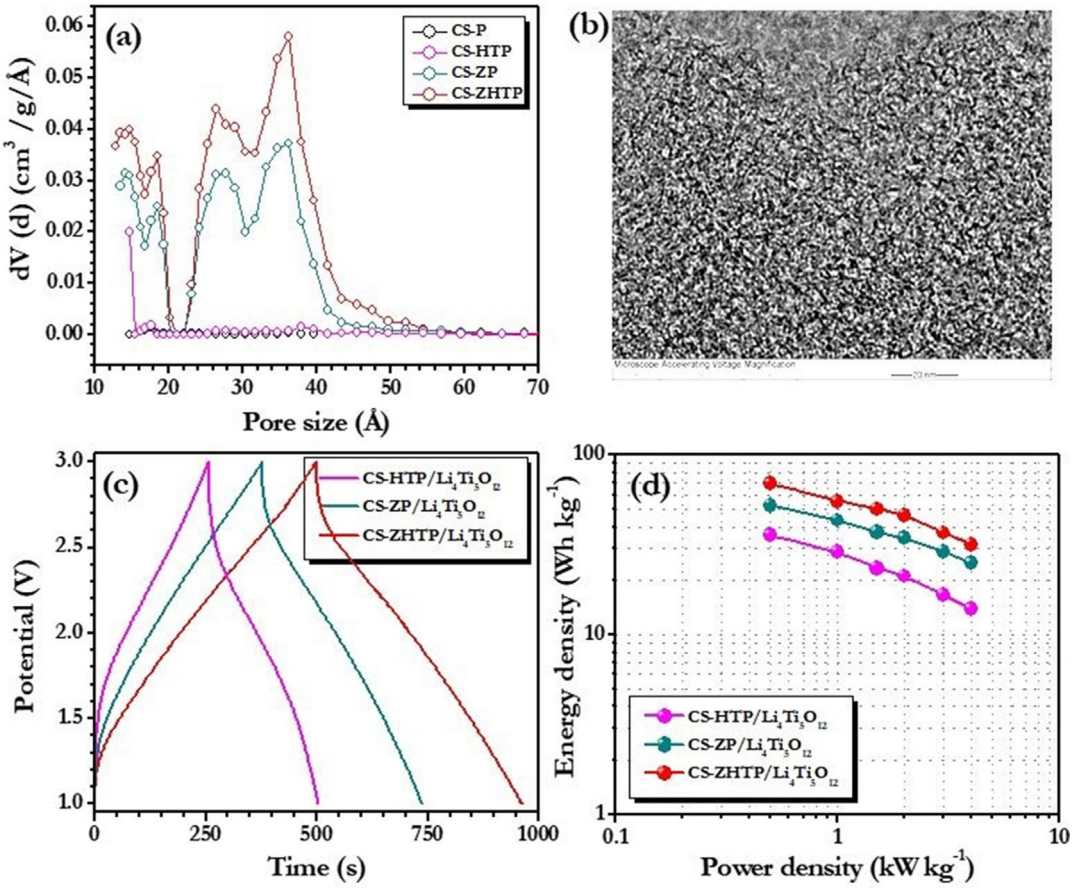

Figure 1. a) Pore-size distributions of coconut-shell-derived carbon materials; b) TEM images of CS-ZHTP; c) charge–discharge curves of coconut-shell-derived carbon materials vs. $Li_4Ti_5O_{12}$ (current density: 250 mA g^{-1}, applied current is based on total mass loading; electrolyte: 1 M $LiPF_6$ in EC/DMC); and d) Ragone plot. The coconut shells were treated under four different conditions: 1) pyrolyzed activated carbon in the presence of N_2 (CS-P); 2) pyrolysis with $ZnCl_2$ in the presence of CO_2 (CS-ZP; $ZnCl_2$/coconut shell granules ratio: 2:1); 3) successive hydrothermal treatment and pyrolysis of raw coconut shell granules in the presence of CO_2 (CS-HTP); 4) hydrothermal reaction and pyrolysis of coconut shell granules in the presence of CO_2 with the addition of $ZnCl_2$ (CS-ZHTP; $ZnCl_2$/coconut shell granules ratio: 2:1). Reproduced with permission from ref. [59]. Copyright 2013, Nature Publishing Group.

ty (3 kW kg^{-1}) were noted for this assembly, with a smaller ohmic drop.

6. *Prosopis Juliflora*

Prosopis juliflora is an environment-threatening invasive weed that has invaded millions of hectares of land in arid and semi-arid areas of Asia, Africa, Australia, and the Americas. The tree absorbs atmospheric humidity, which subsequently decreases rainfall, whilst the emission of CO_2 is another important concern. Therefore, many countries are actively attempting to remove *P. juliflora*, through the so-called "*Juliflora* tree abolish movement". On the other hand, its wood is dimensionally stable and used predominantly as wood fuel or in construction sites, and it could be a valuable solution to wood shortage, which would lessen the pressure on natural and plantation forests. Along this line, Sennu et al. explored the possibility of using the same wood in a high-performance electrode for LIC capacitors.[63,64] Chemical activation (KOH) was conducted under a N_2 atmosphere, which afforded extremely high porosity. Interestingly, the resultant product exhibited a graphene-like phase, with high surface area (2448 m^2 g^{-1}). Two different LIC configurations were explored, $Li_4Ti_5O_{12}$ and pre-lithiated graphite (LiC_6), with *P. juliflora*-derived carbon (KV-AC) as the counter electrode. KV-AC delivered specific capacitances of about 180 and 167 F g^{-1} in a single-electrode configuration for anion (PF_6^-) and both anion (PF_6^-) and cation (Li^+) adsorption/desorption studies, respectively. Under the optimized conditions, KV-AC delivered energy densities of about 80 (at ca. 0.2 kW kg^{-1}) and 162 Wh kg^{-1} (at 0.15 kW kg^{-1}) for $Li_4Ti_5O_{12}$ and LiC_6, respectively (Figure 2). Exceptional behavior was also observed in the cycling profiles, for example, about 76% (10000 cycles) and 79% (7000 cycles) of the initial values were retained when paired with $Li_4Ti_5O_{12}$ and LiC_6 anodes, respectively. The same group also successfully developed a battery-type semi-crystalline carbon (*sc*-KV) electrode from *P. juliflora* wood for an LIC.[65] After changing the wood into char, the black powder was mixed with KOH in a 1:2 ratio (wt./wt.) at 1000 °C for 3 h, which showed a high surface area of 2082.8 m^2 g^{-1} and a total pore volume of 1.34 cm^3 g^{-1}. The internal structure of the resultant product comprised solid and transparent sheet-like carbon materials in a highly disordered structure, and the interlayer spacing in KV-AC (ca. 0.339 nm) corresponded to the d(002) plane of graphitic carbon. At the same time, amorphous carbon with few-layer graphene (*sc*-KV) was prepared without any activation process, but only displayed a surface area of 9.6 m^2 g^{-1} with a hollow-tube-like structure. When *sc*-KV was employed as an anode with KV-AC as a cathode, the fabricated LIC assembly delivered a maximum energy density of about 216 Wh kg^{-1}, with a power density of 155 W kg^{-1} under ambient conditions, as well as about 186 Wh kg^{-1} at 55 °C. Furthermore, the LIC presented outstand-

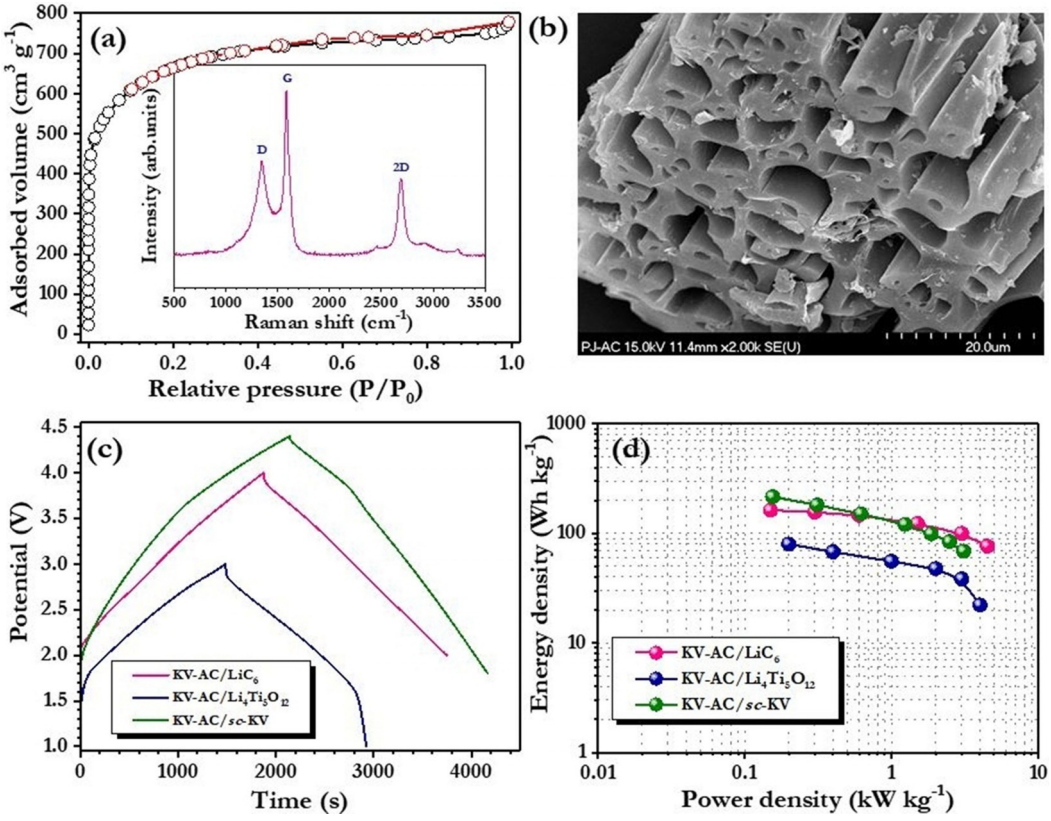

Figure 2. BET specific analysis: a) N_2-adsorption/-desorption isotherms of KV-AC (inset: Raman spectrum); b) SEM image; c) galvanostatic charge–discharge curves of KV-AC with LiC_6, $Li_4Ti_5O_{12}$, and *sc*-KV anodes (current density: 0.1 Ag^{-1}; electrolyte: 1 M $LiPF_6$ in EC/DMC); and d) Ragone plot. Reproduced with permission from ref. [65]. Copyright 2019, Elsevier. Reproduced with permission from ref. [63]. Copyright 2016, Elsevier. Reproduced with permission from ref. [64]. Copyright 2016, John Wiley and Sons.

ing cycling performance, with about 94% capacity retention after 5000 cycles at 25 °C, but only about 73% at 55 °C.

7. Neem Leaves

Dead neem (*Azadirachta indica*) leaves (DNL) have also been explored for the preparation of high-surface-area AC (DNL-AC).[66,67] The authors compared the chemical composition of dry and green leaves, and found that dry leaves contained a larger amount of elemental calcium. It is well-known that calcium is a porogen that is used to increase specific surface area. In this case, the dry/dead leaves were calcined at 1000 °C for 4 h under a flow of Ar gas, and the pore-size distribution of DNL-AC clearly revealed the predominant formation of micropores (5–10 Å), whilst mesopores were also observed, along with micropores to a small extent (20 Å). Because no specific post-treatment/activation was performed to increase the surface area of DNL-AC (1230 $m^2 g^{-1}$), it was used directly in the LIC. Furthermore, the interlayer distance was 0.34 nm, based on the number of "onion-like" graphitic layers that could be supported to achieve good conductivity. As a result, NDL-AC delivered a specific capacitance of about 72 $F g^{-1}$, which was marginally lower than that of commercially available AC (CAC; ca. 74 $F g^{-1}$), owing to the participation of more micropores in the adsorption/desorption process through diffusion, because it maintained a high surface-area-to-volume ratio. Mesopores also provided broader transport channels compared to micropores for high adsorbate penetrability. As expected, the energy density was more or less the same as that of CAC (ca. 35 $Wh kg^{-1}$) at low power (0.5 $kW kg^{-1}$). However, at high power (4 $kW kg^{-1}$), the energy density of the NDL-AC-based LIC was almost 1.5-times higher (ca. 15 $Wh kg^{-1}$) compared to CAC (ca. 10 $Wh kg^{-1}$).

8. Shredded Paper

Shredded paper (SP) is one of the most common forms of waste across the world. Puthusseri et al. explored the possibility of recycling SP as a prospective electrode for the fabrication of a high-energy carbonaceous material (SP-AC) for LIC assemblies with a commercial $Li_4Ti_5O_{12}$ anode.[68] High-surface-area carbon was obtained following hydrothermal carbonization in the presence of 1 M H_2SO_4 and subsequent activation with KOH in a 1:2 ratio at 800 °C for 4 h under a flow of Ar gas. Furthermore, XRD analysis confirmed the presence of the (002) plane of graphite in the resultant material and Raman analysis established partial graphitization, based on the position of the peak relating to the D band at 1315 cm^{-1}, which was not detected in pure graphite. The specific surface area was about 2341 $m^2 g^{-1}$, with a wide range of porosity, that is, meso-, micro-, and macroporous morphologies. Furthermore, the size of the mesopores was within the range 2–3 nm and the total pore volume was 1.1 $cm^3 g^{-1}$, based on DFT calculations. SP-AC delivered a specific capacitance of about 158 $F g^{-1}$ in a single-electrode configuration with lithium. When the SP electrode was paired with spinel $Li_4Ti_5O_{12}$, the LIC displayed a maximum energy density of about 61 $Wh kg^{-1}$ at 0.5 $kW kg^{-1}$. Moreover, an excellent power density of 10 $kW kg^{-1}$ was observed for this LIC, with an energy density of 13 $Wh kg^{-1}$. Good cyclability was also noted for such an interesting configuration: for example, about 85% of the energy density was retained after 5000 galvanostatic cycles (Figure 3). The loss of capacitance was mostly owing to the reaction between the electrolyte and the $Li_4Ti_5O_{12}$ electrode.

9. Teak Wood

Similar to CS-derived carbon materials, Jain et al. attempted to widen the mesoporosity of high-surface-area AC by using teak wood (*Tectona Grandis*; TW) sawdust.[69] The authors employed three strategies to increase the mesoporosity of TW: standard $ZnCl_2$ activation and subsequent pyrolysis (TW-AC-P), hydrothermal activation with H_2O_2 and subsequent pyrolysis (TW-AC-HP), and hydrothermal treatment with H_2O_2 in the presence of benzene tetracarboxylic acid and subsequent pyrolysis (TW-AC-HBP). Specific surface areas of 1738, 1694, and 2108 $m^2 g^{-1}$ and mesoporous areas of 960, 1215 and 1423 $m^2 g^{-1}$ were obtained for TW-AC-P, TW-AC-HP, and TW-AC-HBP, respectively. This study clearly indicated that the porosity could be tailored by altering the synthetic procedure. Furthermore, the I_D/I_G ratios for the as-prepared materials (TW-AC-P, TW-AC-HP, and TW-AC-HBP) were calculated to be about 0.86:1, 0.85:1, and 0.85:1, respectively, whilst their specific capacitances were about 117, 124, and 131 $F g^{-1}$, respectively. Based on its higher specific capacitance, LICs of TW-AC-HBP were fabricated with LiC_6 and $Li_4Ti_5O_{12}$ as anodes under balanced loadings and maximum energy densities of about 111 and 53 $Wh kg^{-1}$ were recorded, respectively, at a power of about 0.15 $kW kg^{-1}$, with good cyclability.

10. Orange Peel

An orange peel (OP)-derived AC (OP-AC) with pre-lithiated graphite and $Li_4Ti_5O_{12}$ was reported by Maharjan et al.[70] Prior to the pre-calcination process, the raw material was ball-milled and calcined at 400 °C to char it. Then, the material was mixed with KOH (1:2 ratio) and sintered at 900 °C under an Ar atmosphere to afford an AC with a very high surface area (ca. 1901 $m^2 g^{-1}$) and type-I and type-IV isotherms, which indicated the presence of both micropores and mesopores. Raman spectroscopy revealed the predominant presence of sp^2-type carbon species, with an I_D/I_G ratio of 0.99:1. The presence of both meso- and microporosity was confirmed by BET and TEM analysis. Moreover, the presence of 22.7% of oxygen-containing functional groups on the OP-AC surface was identified by using X-ray photoelectron spectroscopy (XPS) analysis, which could help to promote electrochemical processes. It is well-known that pre-lithiated graphite and $Li_4Ti_5O_{12}$ function under different conditions and environments. As such, OP-AC had to be tested accordingly, and it was paired with counter electrodes of pre-lithiated graphite and $Li_4Ti_5O_{12}$ in ratios of 4.9:1 and 3.4:1, respectively. The corresponding LICs with $Li_4Ti_5O_{12}$- and pre-lithiated-graphite-based assemblies rendered maximum energy densities of about 35 and 106 $Wh kg^{-1}$, respectively. No-

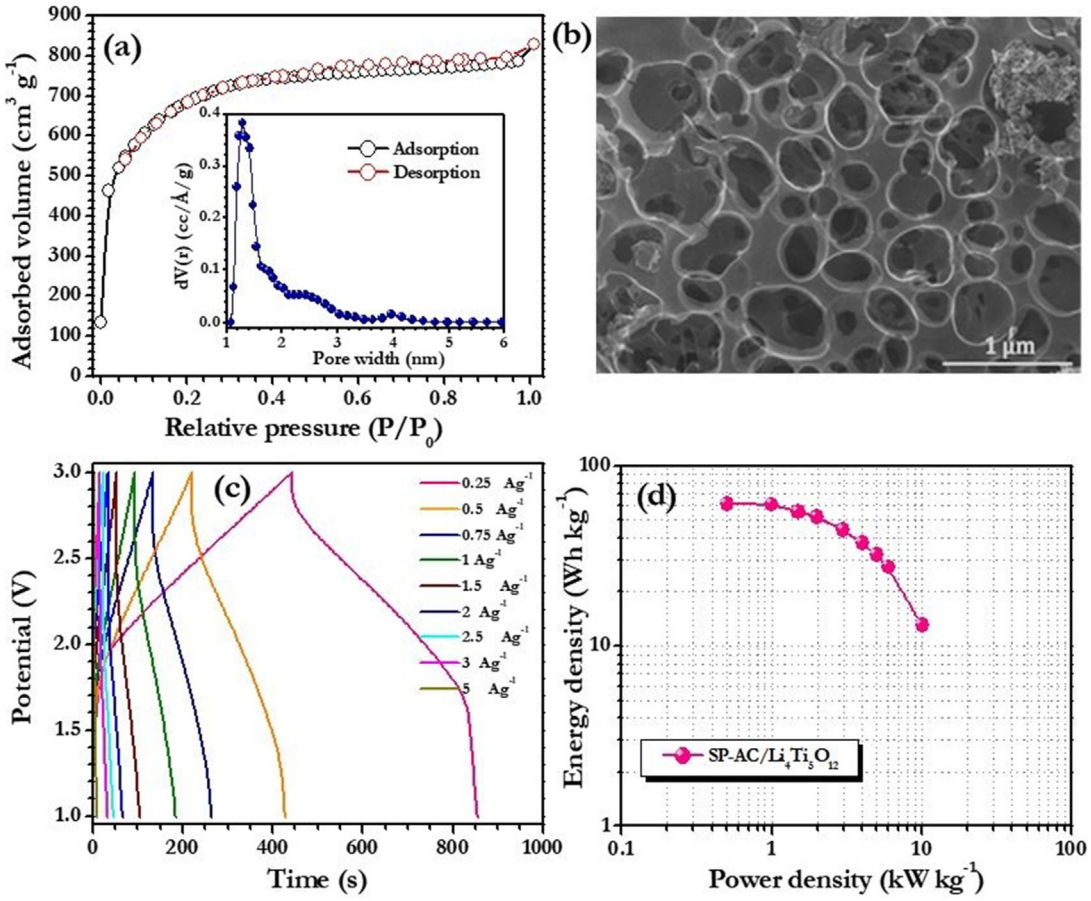

Figure 3. a) N_2-adsorption/-desorption isotherm of SP-AC (inset: pore-size distribution, calculated from the adsorption isotherm by using DFT calculations); b) FE-SEM image of SP-AC; c) galvanostatic charge–discharge curves of a LIC with SP-AC as a cathode and $Li_4Ti_5O_{12}$ as an anode at different current densities; and d) Ragone plot of an SP-AC-based LIC (electrolyte: 1 M $LiPF_6$ in EC/DEC). Reproduced with permission from ref. [68]. Copyright 2014, John Wiley and Sons.

tably, the configuration with OP-AC and pre-lithiated graphite exhibited the highest energy density of about 21 Wh kg^{-1} at a high power density of 5.9 kW kg^{-1}. On the other hand, at high current cycling, the $Li_4Ti_5O_{12}$-based LIC displayed a better cycling profile than LiC_6.

11. Olive Pits

Ajuria et al. reported a synthesis of hard carbon and activated carbon from waste olive pits (O-HC and O-AC, respectively) for the fabrication of high-performance LICs and NICs.[71] Olive pits are composed of 25% α-cellulose, 35% hemicellulose, and 40% lignin, with 50.8% carbon content, a relatively high oxygen content of 42.7%, 7.1% hydrogen content, 0.48% nitrogen content, and 0.04% sulfur content, although the actual content may vary with the quality of the sample. However, this conversion holds the yield of only about 25%. The direct pyrolysis of olive pits at 800 °C for 2 h under a flow of Ar gas allowed the formation of HC, and subsequent mixture of the product with KOH in a 1:6 ratio afforded AC. Pyrolysis treatment ejected the non-carbon elements as tar and gases, thereby shaping a rigid carbon skeleton that consisted of non-graphitic stacked graphene layers, as observed by SEM analysis. Furthermore, the KOH activation triggered the formation of micropores in the graphene layers, which are indispensable for the ion-adsorption process. The thus-obtained AC showed a specific surface area of 2225 m^2 g^{-1}. Half-cell studies revealed that O-HC could act as an excellent insertion host for the reversible accommodation of Li^+ and Na^+ ions. An LIC and an NIC were fabricated with O-AC/O-HC and delivered energy densities of about 100 and 123 Wh kg^{-1}, respectively, along with very good cycling profiles.

12. Corncob

There have been numerous reports on insertion-type materials, such as $Li_4Ti_5O_{12}$, HC, and graphite, as promising electrodes in high-energy-density LICs. Disappointingly, limited lithium-ion kinetics and capacity hamper their ability to achieve high energy densities. Therefore, Yi et al.[72] first explored the possibility of using an alloy-type silicon-based composite (boron-doped Si-SiO_2-C composite) as a negative electrode for LIC applications, which showed much higher theoretical capacity (> 3500 mAh g^{-1}) in a half-cell configuration, with the expected lower working potential (< 0.5 V vs. Li).[73] Similar to the lithiation process for insertion anodes, such as MCMB, HC, and

graphite, a pretreatment step for alloy-type electrodes could also be effectively used to eliminate the irreversible capacity loss (ICL) and for pre-lithiation. Later, Li et al. utilized an alloy-type Si-based composite (Si-C) as an anode with a corncob-derived AC (CC-AC) in an LIC.[74] Chemical activation with KOH (3:1 ratio) in the presence of NH_3/N_2 at various temperatures afforded N_2-doped ACs. Of these materials, CC-AC that was treated at 400 °C delivered the highest specific surface area (ca. 2859 $m^2 g^{-1}$) and capacitance (ca. 182 $F g^{-1}$) with lithium. The authors used fluoroethylene carbonate (FEC; 10%) as an additive with conventional electrolyte (1.2 M $LiPF_6$ in EC/DEC/DMC, 1:1:1 v/v/v; EC = ethylene carbonate, DEC = diethyl carbonate, DMC = dimethyl carbonate), which was essential for stabilizing the silicon-based systems over long-term cycling.[75–77] This CC-AC/Si-C system displayed a maximum energy density of about 230 $Wh kg^{-1}$ at a power of 1.75 $kW kg^{-1}$, with excellent retention (ca. 88%) after 8000 cycles within the range 2–4.5 V. Furthermore, this device delivered an energy density of 141 $Wh kg^{-1}$ at a high power density of 30.13 $kW kg^{-1}$. The same group also attempted to pair CC-AC with an insertion-type $Li_4Ti_5O_{12}$ anode with various mass loadings,[78] of which a 1:1.5 ($Li_4Ti_5O_{12}$/CC-AC) loading registered a maximum energy density of about 75.9 $Wh kg^{-1}$ with good cycling properties.

13. Pomelo Peel

Sun et al. reported rationally designed Sn-C composites as negative electrodes with pomelo-peel-derived AC (PAC) as the cathode.[79] In this approach, the influence of activation temperature (700–900 °C) was studied with KOH as an activating agent in a 1:4 ratio under a flow of N_2 gas. Thus, smooth carbon sheets of PAC were formed at 900 °C (PAC-900), with a small thickness of tens of microns. As well as the sheet structure, a stacked-graphene structure was also observed, as certified by TEM analysis. The presence of stacked-graphene layers was further confirmed by Raman spectroscopy, which showed a characteristic peak for the 2D band at about 2700 cm^{-1}. Furthermore, this highly graphitic structure may improve the electronic conductivity and rate performance. The presence of a type-I isotherm established the predominance of micropores in PAC-900. Moreover, Sn-C was prepared by infiltrating a nitrogen-rich porous carbon framework with $SnCl_2$ solution. The framework was subsequently subjected to calcination and very high reversibility, even higher than the theoretical capacity of Sn, was noted for the Sn-C composite electrode in a half-cell configuration. As usual, the Sn-C composite electrode was also pre-lithiated then and paired with PAC-900. Of the PAC materials that were tested, PAC-900 delivered the best capacitive behavior, with a specific surface area and pore volume of 2167 $m^2 g^{-1}$ and 0.98 $cm^3 g^{-1}$, respectively. An LIC was fabricated with pre-lithiated Sn-C as a negative electrode and PAC-900 as a cathode in a 1:3 ratio. Interestingly, the LIC was tested up to 4.5 V, which led to a high energy density of 195.7 $Wh kg^{-1}$ at a power of 0.73 $kW kg^{-1}$, with an excellent cycling profile and 70% retention after 5000 cycles. Importantly, this cell sustained a laudable energy density of about 84.6 $Wh kg^{-1}$, even at a high power density of 24.34 $kW kg^{-1}$.

14. Hemp Bast Fiber

To date, the scope of suitable conversion-/displacement-type materials for secondary lithium-ion battery applications as anodes is very limited, owing to their huge polarization, large irreversible capacity loss, and poor cyclability. However, two of these issues can now be easily addressed by using pretreatment and by forming composites with active or inactive materials. However, polarization remains an issue that hinders the construction of practical lithium-ion cells. As a result, conversion-type electrodes are considered to be "showcase anodes" and research activity in this area is purely from an academic perspective.[73,80] On the other hand, the slightly elevated redox potentials of such anodes (> 0.5 V vs. Li) favor their use as negative electrodes in LIC assemblies, along with high-surface-area carbonaceous electrodes. The wider working potentials of LICs, that is, 2–4 V, 2–4.5 V, or 1.5–4 V, offsets large polarization, which is induced during the metal formation and reverse reaction. However, the slightly elevated redox potential of conversion electrodes minimizes the possible lithium plating at high currents, compared to alloying (Si, Sn, Ge, etc.,) and insertion-type electrodes (graphite, hard carbon). Along this line, Wang et al. reported the use of ACs that were derived from hemp bast fiber (HBF) with a 3D architecture as cathodes and their composites with MnO as anodes (MnO-HBF-AC).[81] HBF-AC was obtained by hydrothermal treatment and chemical activation with KOH in a 1:1 ratio at 850 °C under a flow of Ar gas. The resultant HBF-AC showed a maximum specific surface area and capacitance (vs. Li) of about 2260 $m^2 g^{-1}$ and 168 $F g^{-1}$, respectively. When HBF-AC was paired with MnO-HBF, a maximum energy density of about 184 $Wh kg^{-1}$ was obtained at 0.08 $kW kg^{-1}$ between 1–4 V (Figure 4). Furthermore, the authors also explored various anode/cathode mass loadings (1:1, 1:2, 1:4, 1:6, and 1:8) to afford higher energy densities, and a 1:2 ratio afforded the energy density mentioned above. As expected, narrowing the potential range from 1–4 to 1–3.5 V resulted in dilution of the energy density, but improved the retention characteristics; for example, about 76 and 81% of the initial values were recorded after 5000 cycles for potential windows of 1–4 to 1–3.5 V, respectively.

15. Kapok Fiber

Zhao et al. reported the performance of 2D kapok fiber (KF)-derived ACs as a positive electrode and KF-based MnO as A negative electrode for high-energy LICs.[82] A high specific surface area (2056 $m^2 g^{-1}$) with a 2D morphology was realized for KF-AC on calcination at 900 °C under a nitrogen atmosphere with 1:5 ratio of KOH. A nanosheet structure with a large number of pores was observed for KF-AC, based on TEM analysis, and it displayed a partially graphitic structure, with an interlayer distance of 0.35 nm. In addition, XPS analysis supported the presence of carbon and nitrogen atoms in KF-AC, which offered extra active sites for ion storage. To prepare composites with MnO, the KF was first fired at 1500 °C and then treated with HNO_3 to further disperse it in the $KMnO_4/K_2SO_4$ solution. Then, the obtained sample was calcined at 500 °C under

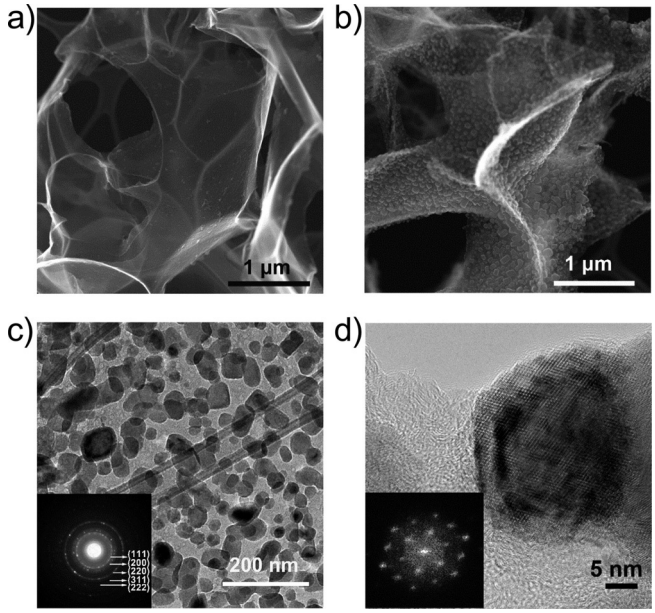

Figure 4. a) SEM image of HBF-AC; b) low-magnification SEM images of 3D MnO-HBF-AC; c) bright-field TEM image of 3D MnO-HBF-AC (inset: indexed selected-area electron diffraction (SAED) image); and d) high-resolution TEM image of a MnO nanocrystallite in 3D MnO-HBF-AC that was oriented in the [110] zone axis (inset: associated fast Fourier transform image). Reproduced with permission from ref. [81]. Copyright 2014, American Chemical Society.

an inert atmosphere for 5 h. The uniform distribution of MnO_2 nanocrystals over the surface of the carbon nanosheets (thickness: ca. 350 nm) was evidenced by SEM and TEM analysis. Furthermore, a high specific surface area of 157 $m^2 g^{-1}$ was achieved for this composite, with a total pore volume of 0.20 $cm^3 g^{-1}$. Pore-size-distribution analysis showed that 72.8% of the mesopores were larger than 2 nm in the MnO-C composite, which helped to achieve outstanding electrochemical performance. Reversible capacities of about 506 and 51 mAh g^{-1} were obtained at a current density of 0.1 A g^{-1} for MnO-C and KF-AC, respectively. In this case, the MnO would undergo a conversion reaction during the charge–discharge process, whereas KF-AC involved a physisorption process. Various mass loadings of the pre-activated MnO-C were used during the fabrication of the LICs, of which a 1:2 ratio (MnO-C/KF-AC) delivered the highest energy density of about 100 Wh kg^{-1} at a power density of about 83 W kg^{-1}. In addition, this LIC exhibited energy and power densities of 30 Wh kg^{-1} and 20 kW kg^{-1}, respectively, at a discharge time of 5 s.

16. Peanut Shell

There have been many reports on the efficient utilization of biomass-derived carbon materials as prospective electrodes for LIC applications. In the same fashion, there have been a few reports on the corresponding NIC applications. For instance, Ding et al. reported the first complete utilization of peanut shell (PS)-derived carbon as positive (activated carbon, PS-AC) and negative electrodes (hard carbon, PS-HC) in NIC assemblies.[83] They activated the outer rough part of PS through hydrothermal and subsequent KOH treatment (1:3 ratio) at 800 °C (under a flow of Ar gas) to prepare the positive electrode (PS-AC). On the counter side, an inner soft part of PS was graphitized at 1200 °C and consequent mild activation in air (300 °C) afforded the ordered carbon, that is, hard carbon (PS-HC). PS-AC displayed a very high specific surface area of about 2396 $m^2 g^{-1}$, with about 35% mesoporosity. The hydrothermal carbonization process led to the presence of active functional groups on the positive electrode, and exhibited a specific capacitance of about 213 F g^{-1} with a sodium electrode. On the other hand, PS-HC delivered a reversible capacity of about 290 mAh g^{-1} at low current rates. Although there were no clear differences between the electrochemical profiles of activated (mild activation in air) and unactivated PS-HC at low current rates, a clear difference was evident at high current rates. Mild activation in air clearly increased the specific surface area (78 to 476 $m^2 g^{-1}$) by diluting the mesoporous nature from 55% to 22%. Therefore, the improved electrochemical activity of PS-HC was evident, which would be beneficial for realizing high power capability. The net NIC delivered a maximum energy density of about 201 Wh kg^{-1} at 0.29 kW kg^{-1}, which is one of the highest reported energy densities for either LICs or NICs.[16,84] Furthermore, all of the PS-based NICs delivered exceptional cyclability, irrespective of the operation at ambient (25 °C) or elevated (65 °C) temperature; for instance, about 88 and 78% of the initial values were retained after 100 000 cycles at ambient and elevated temperatures, respectively. Dong et al. also explored the possibility of using PS-AC as a positive electrode with $Na_2Ti_3O_7$@CNT (CNT = carbon nanotubes) coaxial nanocables in NIC assemblies.[85] A dramatic improvement in the electrochemical performance of NICs was noted. PS-AC/$Na_2Ti_3O_7$@CNT NIC delivered a maximum energy density of about 59 Wh kg^{-1} at a power capability of 0.3 kW kg^{-1}, much higher than that of the CAC/$Na_2Ti_3O_7$ system reported previously.[86,87] Besides a commendable energy density of 21.6 Wh kg^{-1} at 3 kW kg^{-1}, the PS-AC/$Na_2Ti_3O_7$@CNT system rendered excellent cyclability for up to 4000 cycles, with 75% retention of the initial value. Dong et al. also studied the electrochemical activity of PS-AC with Ti^{3+}-doped $Li_4Ti_5O_{12}$ as a counter electrode, in which PS-AC was prepared by using a standard synthetic process with KOH activation in a 1:3 ratio at 800 °C under a flow of Ar gas.[88] This PS-AC/Ti^{3+}-doped $Li_4Ti_5O_{12}$-based LIC delivered a maximum energy density of about 67 Wh kg^{-1} at 0.5 kW kg^{-1} for 5000 cycles, with a retention of about 80%. Furthermore, even at an extreme power density of 8 kW kg^{-1}, this LIC exhibited a creditable energy density of 28.5 Wh kg^{-1}.

17. Cotton Stalk

Chen et al. explored and compared the electrochemical performances of ACs that were derived from a variety of biomass precursors: peanut shells, wheat straw, rice straw, corn stalks, cotton stalks (COT), and soybean stalks (Figure 5).[89] These precursors were charred by using a hydrothermal approach and subsequently activated with KOH (1:3 ratio) at 800 °C under a flow of Ar gas. It is well-known that the hydrothermal charring process enables the presence of active functional groups on

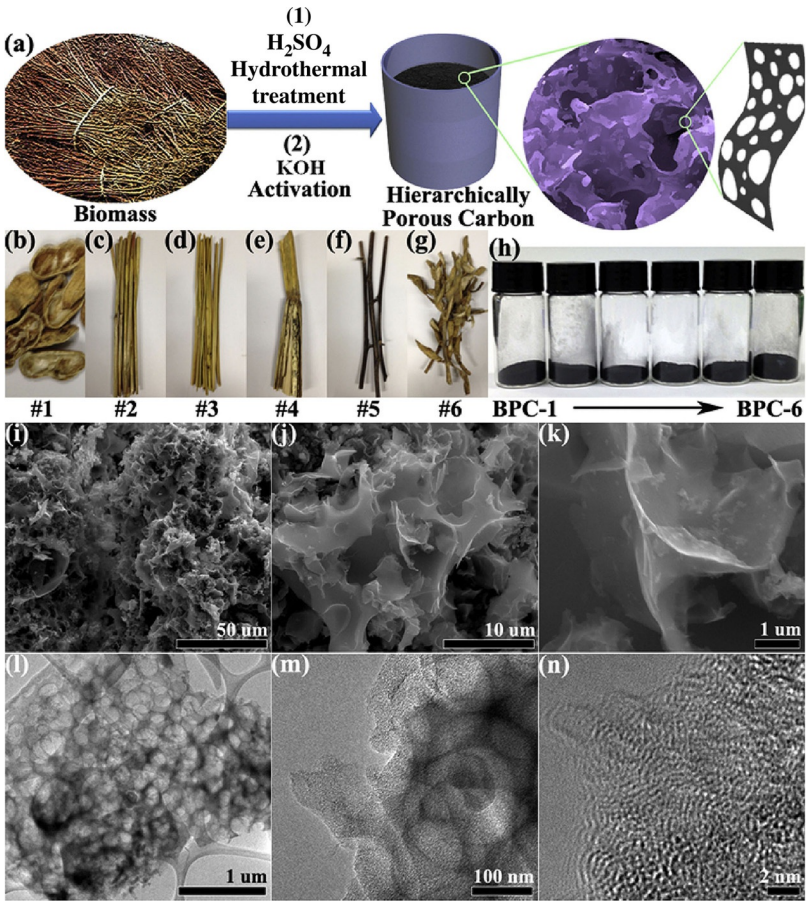

Figure 5. a) Schematic representation of the synthesis of biomass-derived hierarchically porous carbon materials. b–h) Optical photographs of different biomass precursors, peanut shell (#1; b), wheat straw (#2; c), rice straw (#3; d), corn stalk (#4; e), cotton stalk (#5; f), soybean stalk (#6; g), and the corresponding carbon products (h), namely peanut shell, wheat straw, rice straw, corn stalk, cotton stalk, and soybean stalk, respectively. i–n) SEM images (i–k) and TEM images (l–n) of BPC-5.Reproduced with permission from ref. [89]. Copyright 2019, Elsevier. BPC = biomass precursor.

the surface, which triggers the realization of higher specific capacitance. All of the resulting materials exhibited very high specific surface areas of above 1500 $m^2 g^{-1}$. Prior to the fabrication of the NICs, all of the carbonaceous materials were screened in a half-cell configuration with sodium. Among the various AC carbon materials that were prepared, a cotton-stalk-derived AC rendered the highest specific capacitance and highest power capability. Then, the NIC was fabricated with insertion-type, micron-sized $Na_2Ti_{2.97}Nb_{0.03}O_7$, with active mass loadings from 1.2:1 to 1.3:1 with respect to the biomass-derived AC (COT-AC). The NIC delivered a maximum energy density of about 169.4 Wh kg^{-1} at a specific power of 0.12 kW kg^{-1} with limited cycling profiles. Still, the NIC delivered an energy density of 30 Wh kg^{-1} when the power density was increased to an extreme value (1.87 kW kg^{-1}).

18. Cinnamon Stick

Cinnamon sticks are an important spice in Indian cuisine and are predominantly used as flavorings for preparing dishes. Although they have a long history in traditional medicine, there is still no scientific evidence of their use in treating any medical conditions. Based on the origin of the plant, cinnamon has been categorized as Ceylon cinnamon and used to prepare ACs for applications in charge-storage devices. High-surface-area carbonaceous materials have been obtained by treating the charcoal of cinnamon sticks with KOH in a 1:5 ratio at 650 °C for 1.5 h under an Ar atmosphere.[90] The resultant AC (CN-AC) exhibited a specific surface area of 1540 $m^2 g^{-1}$ and displayed a specific capacitance of about 135 F g^{-1} in a single-electrode configuration with sodium metal. Carbon-coated $Na_3V_2(PO_4)_3$ was prepared and employed as a negative electrode in an NIC assembly. The CN-AC/$Na_3V_2(PO_4)_3$ configuration displayed a very high energy density of about 118 Wh kg^{-1} at a power density of 0.095 kW kg^{-1}, with excellent retention characteristics; for example, about 95% of the initial value was retained after 10000 galvanostatic cycles. To date, this is the highest reported energy density for metal-oxide-based lithium- and sodium-insertion hosts (which include phosphates and silicates, among other structures) that have been studied versus high-surface-area carbonaceous counter electrodes.

19. Egg White

Li et al. attempted to exploit the use of egg-white-derived activated carbon (EW-AC) following chemical treatment with KOH in LIC applications.[91] The chemical treatment process was performed at different temperatures, and the EW-AC that was treated at 900 °C delivered better anion-adsorption/-desorption characteristics compared to the materials that were treated at other temperatures, with a specific surface area of about 3250 $m^2 g^{-1}$, which guaranteed higher capacitance and excellent rate performance for the corresponding LICs. Furthermore, the presence of a type-I isotherm revealed the presence of micropores in the AC and their size was within the range 0.5–2 nm. The EW-AC material that was treated at 900 °C was composed of 96.42% carbon, 0.47% nitrogen, and 3.08% oxygen. Then, the EW-AC paired with a pretreated Si-C composite in an LIC assembly, which was capable of delivering a maximum

energy density of about 257 Wh kg^{-1} at a power density of 0.87 kW kg^{-1}, along with notable cycling profile of 15 000 cycles with about 79.2% retention. This value was improved to 86% by decreasing the upper cut-off potential from 4.5 to 4 V; however, the energy density dropped to 177 Wh kg^{-1}, with a power capability of 0.8 kW kg^{-1}. This greater electrochemical performance of the LIC was mostly attributed to the outstanding features of the EW-AC, such as good electronic conductivity, large specific surface area, predominant microporosity, partial graphitization, and a higher number of oxygen functional groups on its surface. However, the egg white-derived activated carbon materials (EW-NaCl) had a deficiency of macropores and mesopores, which led to a small ion-diffusion distance, as well as encouraged the development of an electric double layer.[92,93] Keeping these shortcomings in mind, Shi et al. derived an EW-NaCl with a combination of micro-, meso-, and macropores, with sizes from about 150 nm to several micrometers, by using NaCl as a macropore-generating template with KOH activation.[94] First, the protein was diluted and mixed with NaCl to obtain a xerogel through freeze-drying. This step was followed by carbonization at 700 °C. Then, KOH was employed to activate the pyrolyzed product at 700 °C under an Ar atmosphere, which afforded a high specific surface area of 3898 m^2 g^{-1}. The N_2-adsorption/-desorption isotherms confirmed the presence of micropores and mesopores, by displaying a hysteresis loop at $P/P_0 > 0.5$. In addition, the anode material, conversion-type Fe_3O_4@C, was also prepared by hydrothermal treatment, followed by annealing at 600 °C.[95–98] Apart from the creation of macropores, NaCl facilitated the enhancement of the degree of graphitization as a graphitic catalyst, which led to a high specific capacity of 119 mAh g^{-1}. Furthermore, the device with the EW-NaCl/Fe_3O_4@C configuration at an optimized ratio of 2:1 demonstrated a specific capacity of 42 mAh g^{-1}, based on the mass loading of the cathode. In addition, the hybrid device bestowed good cycling stability, with capacity retention of 88.3% after 2000 cycles. The superior energy density of 124.7 Wh kg^{-1} from the high power density of 2547 W kg^{-1} was mainly attributed to the good surface area, high degree of graphitization, in-situ-doped heteroatoms, and porous structure of the EW-NaCl (Figure 6).

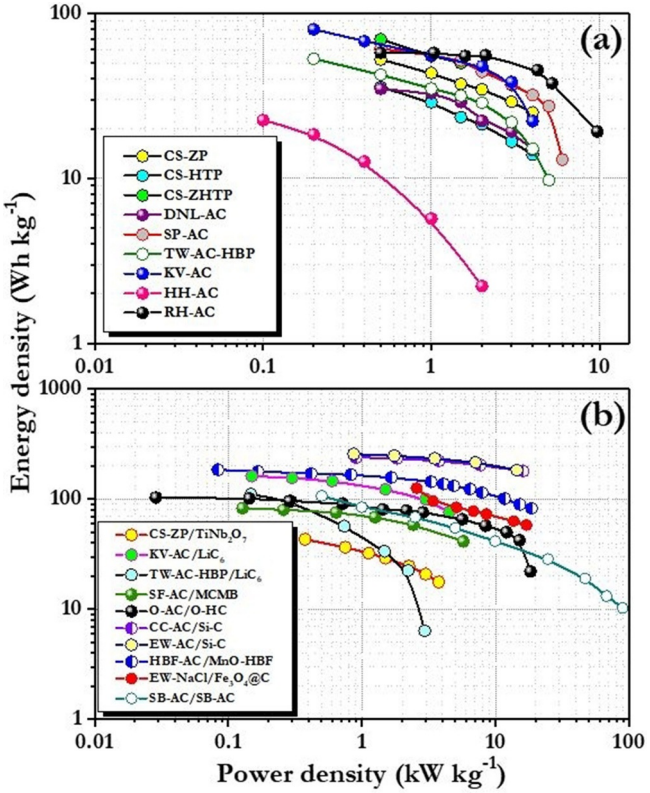

Figure 6. Comparison of various biomass-derived active materials in LIC assemblies. a) Biomass-derived AC materials with an insertion-type $Li_4Ti_5O_{12}$ anode in LICs: CS-ZP, CZ-HTP, and CS-ZHTP,[59] DNL-AC,[67] SP-AC,[68] TW-AC-HBP,[69] KV-AC,[63] HH-AC,[99] and RH-AC.[44] b) LICs based on biomass-derived AC, HC, and composites: CS-ZP/$TiNb_2O_7$,[62] KV-AC/LiC_6,[64] TW-AC-HBP,[69] SF-AC/MCMB,[52] O-AC/O-HC,[71] SB-AC/SB-AC,[102] CC-AC/Si-C,[74] EW-AC/Si-C,[91] EW-NaCl/Fe_3O_4@C,[94] and HBF-AC/MnO-HBF-AC.[81]

20. Human Hair

Satish et al. reported the possibility of using human-hair-derived high-surface-area AC (HH-AC) as a promising electrode for LICs.[99] The use of HH as an AC source is highly beneficial, owing to the presence of keratin (protein), which is inbuilt in the long chains of amino acids that are broken down in the carbonization process to produce residual nitrogen species. Consequently, the resultant carbon material could contain doped nitrogen species, which would increase the carbon conductivity by acting as an electron donor. Furthermore, it is well-known that N-doping can effectively improve the conductivity of the carbon material.[100,101] Moreover, HH also can be prepared chemically. In this case, macroporous HH-AC has been prepared by the activation of NaOH at 750 °C for 3 h under an Ar atmosphere from material collected in barber shops. After carbonization, the thus-obtained material was subjected to XPS analysis to confirm the presence of carbon and self-N-doping. A high surface area of about 1116 m^2 g^{-1} was noted for HH-AC, with a predominant pore-size distribution within the range 100–200 nm. Furthermore, a specific capacitance of about 115 F g^{-1} was observed in a single-electrode configuration with metallic lithium. Interestingly, although a higher specific capacitance was noted for HH-AC compared to CAC, it failed to translate such higher values when paired with spinel $Li_4Ti_5O_{12}$ in LIC assemblies; for instance, a maximum energy density of about 23 Wh kg^{-1} and a power density of 2 kW kg^{-1} were observed, compared to CAC (ca. 35 Wh kg^{-1}). However, good cyclability of 1000 cycles was reported for this LIC. The high specific capacitance for HH-AC was mainly credited to the NaOH activation, which permitted the pore size to increase with the aim of penetrating the solvated ions for the facile adsorption/desorption process.

21. Sheep Bone

High-defect mesoporous carbon was synthesized by Niu et al. from the direct pyrolysis of sheep bones (SB-AC).[102] It is well-known that sheep bones are predominantly composed of col-

lagen and hydroxyapatite, $Ca_x(PO_4,CO_3)_y(OH)$, in which both phosphate and calcium moieties act as pore-generating agents, thereby leading to the formation of highly porous carbonaceous materials. The authors calcined the sheep bones at a relatively high temperature of 1100 °C under a flow of Ar gas, which eventually resulted in the development of meso-/micropores. The existence of O-containing functional groups was validated by XPS studies. The derived carbon material exhibited type-I/type-IV isotherms, which confirmed the occurrence of micropores and mesopores. Furthermore, most of the pores were about 4 nm in size, based on pore-size-distribution and TEM analysis, whilst a very small number of pores were larger than 20 nm. This dominance of mesoporosity in the carbon material was attributed to the in-situ co-activation of steam and CO_2 at 1100 °C, which paved the way for the formation of more micropores than mesopores. Furthermore, the specific surface area and total pore volume for the resultant material were calculated to be 2192 $m^2 g^{-1}$ and 1.99 $cm^3 g^{-1}$, respectively. Capacities of about 109 and 1550 mAh g^{-1} were recorded at a current density of 0.2 A g^{-1} for the positive and negative electrodes, respectively. An SB-AC-based LIC was fabricated based on the optimized anode/cathode ratio of 1:4 and rendered a maximum energy density of about 106.4 Wh kg^{-1} at a power density of 0.5 kW kg^{-1}. Furthermore, good cycling profiles were also evidenced by this fascinating configuration. The same group performed a similar study on the pyrolysis of cattle bones at 550 °C under a flow of Ar gas with a KOH ratio of 1:1.4 and subsequent acid wash to remove the metallic impurities.[103] In this case, the authors studied the influence of hydroxy apatite on the formation of 3D/2D hybrid structures, along with the role of KOH. Among the prepared samples, a carbonaceous material that was prepared with KOH and hydroxyapatite (HPCNS) rendered good sodium-storage capabilities. Furthermore, HPCNS was treated at 800 °C to further asses its sodium-storage properties, which not only removed the surface functionalities, but also narrowed the interlayer distance between the two graphene layers. As a result, the sodium-intercalation properties were severely affected. In other words, the surface only influenced the sodium-storage properties, as was clearly evident from the XPS studies and, of course, galvanostatic studies. Nevertheless, this kind of surface-storage properties eventually increased the high power capability to the system compared to the traditional topotactic insertion behavior. Then, the material was paired with a hierarchical porous carbon (HPC) material that was derived from cattle bones with a specific surface area of 2520 $m^2 g^{-1}$.[104] The HPC/HPCNS-based NIC rendered a maximum energy density of about 105.2 Wh kg^{-1} at 0.07 kW kg^{-1}, with good cycling of 4000 cycles.

22. Outlook and Perspectives

Biomass-derived ACs have displayed excellent electrochemical profiles, irrespective of the insertion host and system that is adopted (LIC or NIC). Apart from high specific surface area, many other factors are involved in enhancing the electrochemical activity of a system, such as pore-size distribution, tailored porosity (meso-, micro-, and macropores), the presence of active functional groups (hydroxy, oxalic, etc.), heteroatom doping (S, Ca, N_2, B, etc.), activation procedure (steam, chemical, physical, hydrothermal, etc.), sintering temperature (> 600 °C), atmosphere (Ar, N_2, CO_2, etc.), choice of substrate (current collector; Al, Cu, Ni foam, stainless steel, carbonaceous paper, polymer, etc.), redox additive, mass loading, and potential window (see the Supporting Information, Table S1).[105] Therefore, it is a little difficult to pinpoint whether the excellent performance of LICs or NICs is owing to the use of biomass-derived ACs if we ignore the properties of the counter electrode. Nevertheless, half-cell/single-electrode performance is an appropriate way of studying the behavior of these biomass-derived materials. Most of the ACs described herein delivered specific capacitances of > 100 F g^{-1} with metallic substances in a single-electrode configuration, which is much better than commercially available AC. Besides high specific surface area, increasing the mesoporosity improves the capacitive properties of these materials, which allows the facile penetration of an electrolyte solution and eventually leads to the formation of a double layer across the interface. In fact, the increase in mesoporosity eventually dilutes the electrical conductivity of the AC and leads to a decrease in the specific capacitance and high power capability; for example, Jain et al. attempted to create high mesoporosity from TW-AC by adopting various procedures, but they only found marginal improvement, and the same behavior was reflected in the LIC assembly.[69] Hence, optimum mesoporosity is sufficient to afford a high-performance configuration.

Heteroatom doping is an inherent feature of biomass-derived carbon materials that improves their electrochemical performance. In this regard, KV-AC is an excellent example of the beneficial effects of heteroatom doping. KV-AC is composed of S and Ca as inherent heteroatoms and displays a specific capacitance of about 180 F g^{-1}. Recently, the hydrothermal treatment of biomass precursors has become attractive, because it leaves active functional groups on the carbonaceous material surface, apart from the char formation. The effect of hydrothermal treatment was investigated by using CS-AC in both single-electrode and LIC assemblies with a $Li_4Ti_5O_{12}$ anode, and chemical treatment after the hydrothermal reaction led to much better electrochemical activity than the individual treatments alone (i.e. activation). During hydrothermal activation, the inclusion of a processing agent allows the mesoporosity to be controlled/tuned to meet particular requirements (Figure 6). Disappointingly, very limited studies are available on the utilization of insertion-type carbonaceous materials, such as HCs from biomass precursors, for either NICs or LICs. Nevertheless, many reports are available from the perspective of lithium-ion batteries (LIBs) and sodium-ion batteries (NIBs) as high-capacity anodes. It is apparent that the mild activation of HC in air promotes higher current performance compared to bare HC that is obtained from pyrolysis during the Faradaic reaction. This property was clearly exemplified for PS-HC during a sodium-insertion/-extraction reaction.

Graphite is an excellent insertion host for battery components, but suffers a lot during high current operation, similar

to LIBs. Although the direct intercalation of sodium ions is not possible, the insertion of sodium ions with solvent molecules is considered to be the perfect choice as an intercalation host (Figure 7). Realizing high power capability is one of the primary

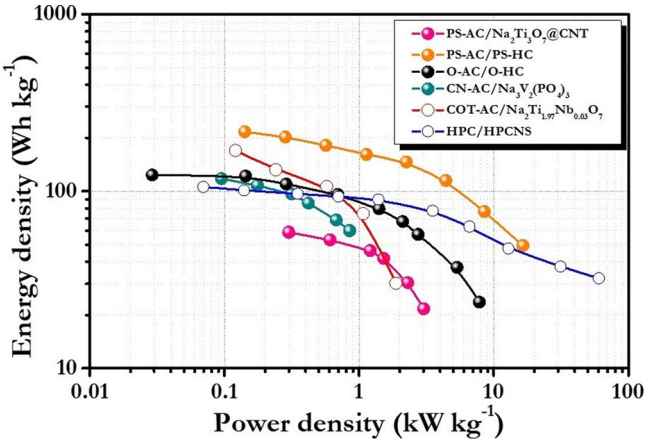

Figure 7. Comparison of various biomass-derived active materials in NIC assemblies: CN-AC/$Na_3V_2(PO_4)_3$,[90] PS-AC/PS-HC,[83] PS-AC/$Na_2Ti_3O_7$@CNT,[85] O-AC/O-HC,[71] COT-AC/$Na_2Ti_{2.97}Nb_{0.03}O_7$,[89] and HPC/HPCNS.[103]

goals for hybrid energy-storage devices. In this regard, high-capacity anodes that undergo displacement and alloying-type reactions have been efficiently utilized as promising battery-type components for the fabrication of high-energy, high-power supercapacitors. Silicon is a special kind of alloying anode that exhibits very high capacity and a close working potential to that of the well-established graphite, and its pairing with biomass-derived carbon materials, that is, CC-AC, is expected to provide very high energy densities, similar to that of LIBs. Similarly, conversion-type anodes have a very limited scope in the secondary battery industry, owing to their large polarization; however, in LICs/NICs, there is no such issue, because of their wider testing potential. Typically, such anodes would be prepared as composites with carbonaceous materials; as such, the same biomass-derived carbon materials could be used, which would not only provide stability during the conversion reaction, but also participate in the double-layer formation. This process has been well-realized in HBF-AC-MnO- and HBF-AC-based LICs. A detailed discussion of the possibility of using conversion and alloy-type materials is beyond the scope of this Minireview, but we have discussed it extensively in our recent review.[14]

Overall, the efficient utilization of high-surface-area carbonaceous counterparts with tailored hierarchical porosity (including micro-, meso-, and macropores) improves the energy density of the system, irrespective whether it is a lithium-ion or sodium-ion system.[105] Instead of using native materials, which undergo insertion/conversion/alloying reactions, the formulation of composites with high-surface-area carbonaceous materials provides the dual benefit of Faradaic reactions and double-layer formation. These benefits not only lead to enhanced energy density, but also boost the power capability. Therefore, further research must explore the utilization of biomass-derived carbon materials for realizing high energy density, preferably for the preparation of both battery-type and double-layer-type electrodes, regardless of whether it is a lithium-ion or sodium-ion (or even potassium-ion) configuration. Besides these application perspectives, the utilization of biowaste certainly offers environmental benefits, and allows the recycling of such "useless" material into useful ones, simply described as "waste-to-wealth".

Acknowledgements

V.A. acknowledges financial support from the Science and Engineering Research Board (SERB), a statutory body of the Department of Science and Technology, Government of India, through a Ramanujan Fellowship (SB/S2/RJN-088/2016). YSL gratefully acknowledges the financial support from the Ministry of Trade, Industry & Energy, Republic of Korea (10080314).

Conflict of interest

The authors declare no conflict of interest.

Keywords: biomass · capacitors · carbon · electrochemistry · materials science

[1] F. Béguin, V. Presser, A. Balducci, E. Frackowiak, *Adv. Mater.* **2014**, *26*, 2219 – 2251.
[2] Y. Gogotsi, *MRS Bull.* **2015**, *40*, 1110 – 1121.
[3] J. Zhang, M. Terrones, C. R. Park, R. Mukherjee, M. Monthioux, N. Koratkar, Y. S. Kim, R. Hurt, E. Frackowiak, T. Enoki, Y. Chen, Y. Chen, A. Bianco, *Carbon* **2016**, *98*, 708 – 732.
[4] E. Frackowiak, F. Béguin, *Carbon* **2001**, *39*, 937 – 950.
[5] E. Frackowiak, *Phys. Chem. Chem. Phys.* **2007**, *9*, 1774 – 1785.
[6] P. Simon, P.-L. Taberna, F. Béguin in *Supercapacitors*, Wiley-VCH, Weinheim, **2013**, Chapter 4, pp. 131 – 165.
[7] P. Sennu, V. Aravindan, Y.-S. Lee, *J. Power Sources* **2016**, *306*, 248 – 257.
[8] W. F. Mak, G. Wee, V. Aravindan, N. Gupta, S. G. Mhaisalkar, S. Madhavi, *J. Electrochem. Soc.* **2012**, *159*, A1481 – A1488.
[9] T. Brousse, D. Bélanger, D. Guay in *Supercapacitors*, Wiley-VCH, Weinheim, **2013**, Chapter 8, pp. 257 – 288.
[10] E. Frackowiak in *Supercapacitors*, Wiley-VCH, Weinheim, **2013**, Chapter 6, pp. 207 – 237.
[11] D. Bélanger, T. Brousse, J. W. Long, *Electrochem. Soc. Interface* **2008**, *17*, 49 – 52.
[12] S. Devaraj, N. Munichandraiah, *J. Phys. Chem. C* **2008**, *112*, 4406 – 4417.
[13] V. Aravindan, J. Gnanaraj, Y.-S. Lee, S. Madhavi, *Chem. Rev.* **2014**, *114*, 11619 – 11635.
[14] V. Aravindan, Y.-S. Lee, *J. Phys. Chem. Letters* **2018**, *9*, 3946 – 3958.
[15] J. Ding, W. Hu, E. Paek, D. Mitlin, *Chem. Rev.* **2018**, *118*, 6457 – 6498.
[16] K. Naoi, S. Ishimoto, J.-I. Miyamoto, W. Naoi, *Energy Environ. Sci.* **2012**, *5*, 9363 – 9373.
[17] A. Chaturvedi, P. Hu, V. Aravindan, C. Kloc, S. Madhavi, *J. Mater. Chem. A* **2017**, *5*, 9177 – 9181.
[18] A. Chaturvedi, P. Hu, C. Kloc, Y.-S. Lee, V. Aravindan, S. Madhavi, *J. Mater. Chem. A* **2017**, *5*, 19819 – 19825.
[19] A. Chaturvedi, P. Hu, Y. Long, C. Kloc, S. Madhavi, V. Aravindan, *Scr. Mater.* **2019**, *161*, 54 – 57.
[20] V. Aravindan, M. Ulaganathan, S. Madhavi, *J. Mater. Chem. A* **2016**, *4*, 7538 – 7548.
[21] K. Naoi, W. Naoi, S. Aoyagi, J.-i. Miyamoto, T. Kamino, *Acc. Chem. Res.* **2013**, *46*, 1075 – 1083.
[22] K. Naoi, *Fuel Cells* **2010**, *10*, 825 – 833.

[23] I. Plitz, A. DuPasquier, F. Badway, J. Gural, N. Pereira, A. Gmitter, G. G. Amatucci, *Appl. Phys. A* **2006**, *82*, 615 – 626.
[24] A. D. Pasquier, I. Plitz, J. Gural, F. Badway, G. G. Amatucci, *J. Power Sources* **2004**, *136*, 160 – 170.
[25] G. G. Amatucci, F. Badway, A. Du Pasquier, T. Zheng, *J. Electrochem. Soc.* **2001**, *148*, A930 – A939.
[26] W. Zuo, R. Li, C. Zhou, Y. Li, J. Xia, J. Liu, *Adv. Sci.* **2017**, *4*, 1600539.
[27] H. Wang, C. Zhu, D. Chao, Q. Yan, H. J. Fan, *Adv. Mater.* **2017**, *29*, 1702093.
[28] T. Liu, B. Lee, M. J. Lee, J. Park, Z. Chen, S. Noda, S. W. Lee, *J. Mater. Chem. A* **2018**, *6*, 3367 – 3375.
[29] A. Jain, R. Balasubramanian, M. P. Srinivasan, *Chem. Eng. J.* **2016**, *283*, 789 – 805.
[30] O. Fromm, A. Heckmann, U. C. Rodehorst, J. Frerichs, D. Becker, M. Winter, T. Placke, *Carbon* **2018**, *128*, 147 – 163.
[31] B. Li, J. Zheng, H. Zhang, L. Jin, D. Yang, H. Lv, C. Shen, A. Shellikeri, Y. Zheng, R. Gong, J. P. Zheng, C. Zhang, *Adv. Mater.* **2018**, *30*, 1705670.
[32] L. Wei, G. Yushin, *Nano Energy* **2012**, *1*, 552 – 565.
[33] Y.-P. Gao, Z.-B. Zhai, K.-J. Huang, Y.-Y. Zhang, *New J. Chem.* **2017**, *41*, 11456 – 11470.
[34] J. Wang, P. Nie, B. Ding, S. Dong, X. Hao, H. Dou, X. Zhang, *J. Mater. Chem. A* **2017**, *5*, 2411 – 2428.
[35] H. Lu, X. S. Zhao, *Sustainable Energy Fuels* **2017**, *1*, 1265 – 1281.
[36] J. Deng, M. Li, Y. Wang, *Green Chem.* **2016**, *18*, 4824 – 4854.
[37] T. K. Enock, X. King, C. K. Ondu, A. Pogrebnoi, Y. A. C. Jande, *Int. J. Electrochem.* **2017**, 6453420.
[38] Y. Liu, J. Chen, B. Cui, P. Yin, C. Zhang, *C* **2018**, *4*, 53.
[39] H.-K. Roh, M.-S. Kim, K. Y. Chung, M. Ulaganathan, V. Aravindan, S. Madhavi, K. C. Roh, K.-B. Kim, *J. Mater. Chem. A* **2017**, *5*, 17506 – 17516.
[40] S. Jayaraman, A. Jain, M. Ulaganathan, E. Edison, M. P. Srinivasan, R. Balasubramanian, V. Aravindan, S. Madhavi, *Chem. Eng. J.* **2017**, *316*, 506 – 513.
[41] K. Shiva, P. Singh, W. Zhou, J. B. Goodenough, *Energy Environ. Sci.* **2016**, *9*, 3103 – 3106.
[42] X. Peng, J. Fu, C. Zhang, J. Tao, L. Sun, P. K. Chu, *Nanosci. Nanotechnol. Lett.* **2014**, *6*, 68 – 71.
[43] G. T. K. Fey, Y. D. Cho, C. L. Chen, Y. Y. Lin, T. P. Kumar, S. H. Chan, *Pure Appl. Chem.* **2010**, *82*, 2157 – 2165.
[44] B. Babu, P. G. Lashmi, M. M. Shaijumon, *Electrochim. Acta* **2016**, *211*, 289 – 296.
[45] S. Jayaraman, G. Singh, S. Madhavi, V. Aravindan, *Carbon* **2018**, *134*, 9 – 14.
[46] S. Jayaraman, S. Madhavi, V. Aravindan, *J. Mater. Chem. A* **2018**, *6*, 3242 – 3248.
[47] T. S. D. Kumari, A. J. J. Jebaraj, T. A. Raj, D. Jeyakumar, T. P. Kumar, *Energy* **2016**, *95*, 483 – 493.
[48] T. P. Kumar, T. S. D. Kumari, A. M. Stephan, *J. Indian Inst. Sci.* **2009**, *89*, 393 – 424.
[49] V. Aravindan, M. Ulaganathan, W. C. Ling, S. Madhavi, *ChemElectroChem* **2015**, *2*, 231 – 235.
[50] S. Jayaraman, V. Aravindan, N. Shubha, M. Ulaganathan, S. Madhavi, *Part. Part. Syst. Charact.* **2016**, *33*, 306 – 310.
[51] Z. Yang, H. Guo, X. Li, Z. Wang, J. Wang, Y. Wang, Z. Yan, D. Zhang, *J. Mater. Chem. A* **2017**, *5*, 15302 – 15309.
[52] Z. Yang, H. Guo, X. Li, Z. Wang, Z. Yan, Y. Wang, *J. Power Sources* **2016**, *329*, 339 – 346.
[53] A. Jain, V. Ong, S. Jayaraman, R. Balasubramanian, M. P. Srinivasan, *J. Supercrit. Fluids* **2016**, *107*, 513 – 518.
[54] A. Jain, C. Xu, S. Jayaraman, R. Balasubramanian, J. Y. Lee, M. P. Srinivasan, *Microporous Mesoporous Mater.* **2015**, *218*, 55 – 61.
[55] A. Jain, R. Balasubramanian, M. P. Srinivasan, *Microporous Mesoporous Mater.* **2015**, *203*, 178 – 185.
[56] M. Ulaganathan, A. Jain, V. Aravindan, S. Jayaraman, W. C. Ling, T. M. Lim, M. P. Srinivasan, Q. Yan, S. Madhavi, *J. Power Sources* **2015**, *274*, 846 – 850.
[57] A. Jain, R. Balasubramanian, M. P. Srinivasan, *Chem. Eng. J.* **2015**, *273*, 622 – 629.
[58] A. Jain, S. Jayaraman, R. Balasubramanian, M. P. Srinivasan, *J. Mater. Chem. A* **2014**, *2*, 520 – 528.
[59] A. Jain, V. Aravindan, S. Jayaraman, P. S. Kumar, R. Balasubramanian, S. Ramakrishna, S. Madhavi, M. Srinivasan, *Sci. Rep.* **2013**, *3*, 3002.
[60] http://www.coconutboard.nic.in/charcoal.htm.
[61] T. Aida, K. Yamada, M. Morita, *Electrochem. Solid-State Lett.* **2006**, *9*, A534 – A536.
[62] V. Aravindan, J. Sundaramurthy, A. Jain, P. S. Kumar, W. C. Ling, S. Ramakrishna, M. P. Srinivasan, S. Madhavi, *ChemSusChem* **2014**, *7*, 1858 – 1863.
[63] P. Sennu, H.-J. Choi, S.-G. Baek, V. Aravindan, Y.-S. Lee, *Carbon* **2016**, *98*, 58 – 66.
[64] P. Sennu, V. Aravindan, M. Ganesan, Y. G. Lee, Y. S. Lee, *ChemSusChem* **2016**, *9*, 849 – 854.
[65] P. Sennu, N. Arun, S. Madhavi, V. Aravindan, Y.-S. Lee, *J. Power Sources* **2019**, *414*, 96 – 102.
[66] M. Biswal, A. Banerjee, M. Deo, S. Ogale, *Energy Environ. Sci.* **2013**, *6*, 1249 – 1259.
[67] A. Suryawanshi, M. Biswal, D. Mhamane, P. Yadav, A. Banerjee, P. Yadav, S. Patil, V. Aravindan, S. Madhavi, S. Ogale, *Appl. Mater. Today* **2016**, *2*, 1 – 6.
[68] D. Puthusseri, V. Aravindan, B. Anothumakkool, S. Kurungot, S. Madhavi, S. Ogale, *Small* **2014**, *10*, 4395 – 4402.
[69] A. Jain, S. Jayaraman, M. Ulaganathan, R. Balasubramanian, V. Aravindan, M. P. Srinivasan, S. Madhavi, *Electrochim. Acta* **2017**, *228*, 131 – 138.
[70] M. Maharjan, M. Ulaganathan, V. Aravindan, S. Sreejith, Q. Yan, S. Madhavi, J. Y. Wang, T. M. Lim, *ChemistrySelect* **2017**, *2*, 5051 – 5058.
[71] J. Ajuria, E. Redondo, M. Arnaiz, R. Mysyk, T. Rojo, E. Goikolea, *J. Power Sources* **2017**, *359*, 17 – 26.
[72] R. Yi, S. Chen, J. Song, M. L. Gordin, A. Manivannan, D. Wang, *Adv. Funct. Mater.* **2014**, *24*, 7433 – 7439.
[73] V. Aravindan, Y.-S. Lee, S. Madhavi, *Adv. Energy Mater.* **2015**, *5*, 1402225.
[74] B. Li, F. Dai, Q. Xiao, L. Yang, J. Shen, C. Zhang, M. Cai, *Energy Environ. Sci.* **2016**, *9*, 102 – 106.
[75] K. Fridman, R. Sharabi, R. Elazari, G. Gershinsky, E. Markevich, G. Salitra, D. Aurbach, A. Garsuch, J. Lampert, *Electrochem. Commun.* **2013**, *33*, 31 – 34.
[76] K. Fridman, R. Sharabi, E. Markevich, R. Elazari, G. Salitra, G. Gershinsky, D. Aurbach, J. Lampert, M. Schulz-Dobrick, *ECS Electrochem. Lett.* **2013**, *2*, A84 – A87.
[77] E. Markevich, K. Fridman, R. Sharabi, R. Elazari, G. Salitra, H. E. Gottlieb, G. Gershinsky, A. Garsuch, G. Semrau, M. A. Schmidt, D. Aurbach, *J. Electrochem. Soc.* **2013**, *160*, A1824 – A1833.
[78] B. Li, H. Zhang, D. Wang, H. Lv, C. Zhang, *RSC Adv.* **2017**, *7*, 37923 – 37928.
[79] F. Sun, J. Gao, Y. Zhu, X. Pi, L. Wang, X. Liu, Y. Qin, *Sc. Rep.* **2017**, *7*, 40990.
[80] M. R. Palacín, *Chem. Soc. Rev.* **2009**, *38*, 2565 – 2575.
[81] H. Wang, Z. Xu, Z. Li, K. Cui, J. Ding, A. Kohandehghan, X. Tan, B. Zahiri, B. C. Olsen, C. M. B. Holt, D. Mitlin, *Nano Lett.* **2014**, *14*, 1987 – 1994.
[82] Y. Zhao, Y. Cui, J. Shi, W. Liu, Z. Shi, S. Chen, X. Wang, H. Wang, *J. Mater. Chem. A* **2017**, *5*, 15243 – 15252.
[83] J. Ding, H. Wang, Z. Li, K. Cui, D. Karpuzov, X. Tan, A. Kohandehghan, D. Mitlin, *Energy Environ. Sci.* **2015**, *8*, 941 – 955.
[84] M. D. Stoller, S. Murali, N. Quarles, Y. Zhu, J. R. Potts, X. Zhu, H.-W. Ha, R. S. Ruoff, *Phys. Chem. Chem. Phys.* **2012**, *14*, 3388 – 3391.
[85] S. Dong, L. Shen, H. Li, P. Nie, Y. Zhu, Q. Sheng, X. Zhang, *J. Mater. Chem. A* **2015**, *3*, 21277 – 21283.
[86] J. Yin, L. Qi, H. Wang, *ACS Appl. Mater. Interfaces* **2012**, *4*, 2762 – 2768.
[87] L. Zhao, L. Qi, H. Wang, *J. Power Sources* **2013**, *242*, 597 – 603.
[88] S. Dong, X. Wang, L. Shen, H. Li, J. Wang, P. Nie, J. Wang, X. Zhang, *J. Electroanal. Chem.* **2015**, *757*, 1 – 7.
[89] J. Chen, X. Zhou, C. Mei, J. Xu, S. Zhou, C.-P. Wong, *J. Power Sources* **2017**, *342*, 48 – 55.
[90] R. Thangavel, K. Kaliyappan, K. Kang, X. Sun, Y. S. Lee, *Adv. Energy Mater.* **2016**, *6*, 1502199.
[91] B. Li, F. Dai, Q. Xiao, L. Yang, J. Shen, C. Zhang, M. Cai, *Adv. Energy Mater.* **2016**, *6*, 1600802.
[92] Q. Xia, H. Yang, M. Wang, M. Yang, Q. Guo, L. Wan, H. Xia, Y. Yu, *Adv. Energy Mater.* **2017**, *7*, 1701336.
[93] Z.-S. Wu, Y. Sun, Y.-Z. Tan, S. Yang, X. Feng, K. Müllen, *J. Am. Chem. Soc.* **2012**, *134*, 19532 – 19535.

[94] R. Shi, C. Han, H. Li, L. Xu, T. Zhang, J. Li, Z. Lin, C.-P. Wong, F. Kang, B. Li, *J. Mater. Chem. A* **2018**, *6*, 17057 – 17066.
[95] H.-K. Kim, V. Aravindan, M. H.-K. Roh, K. Lee, M.-H. Jung, S. Madhavi, K. C. Roh, K.-B. Kim, *ChemElectroChem* **2017**, *4*, 2626 – 2633.
[96] A. Suryawanshi, V. Aravindan, S. Madhavi, S. Ogale, *ChemSusChem* **2016**, *9*, 2193 – 2200.
[97] A. Suryawanshi, V. Aravindan, D. Mhamane, P. Yadav, S. Patil, S. Madhavi, S. Ogale, *Energy Storage Mater.* **2015**, *1*, 152 – 157.
[98] M. Biswal, A. Suryawanshi, V. Thakare, S. Jouen, B. Hannoyer, V. Aravindan, S. Madhavi, S. Ogale, *J. Mater. Chem. A* **2013**, *1*, 13932 – 13940.
[99] R. Satish, A. Vanchiappan, C. L. Wong, K. W. Ng, M. Srinivasan, *Electrochim. Acta* **2015**, *182*, 474 – 481.
[100] L. Li, E. Liu, J. Li, Y. Yang, H. Shen, Z. Huang, X. Xiang, W. Li, *J. Power Sources* **2010**, *195*, 1516 – 1521.
[101] Z. R. Ismagilov, A. E. Shalagina, O. Y. Podyacheva, A. V. Ischenko, L. S. Kibis, A. I. Boronin, Y. A. Chesalov, D. I. Kochubey, A. I. Romanenko, O. B. Anikeeva, T. I. Buryakov, E. N. Tkachev, *Carbon* **2009**, *47*, 1922 – 1929.
[102] J. Niu, R. Shao, M. Liu, J. Liang, Z. Zhang, M. Dou, Y. Huang, F. Wang, *Energy Storage Mater.* **2018**, *12*, 145 – 152.
[103] J. Niu, J. Liang, R. Shao, M. Liu, M. Dou, Z. Li, Y. Huang, F. Wang, *Nano Energy* **2017**, *41*, 285 – 292.
[104] M. Dou, D. He, W. Shao, H. Liu, F. Wang, L. Dai, *Chem. Eur. J.* **2016**, *22*, 2896 – 2901.
[105] P. Simon, A. Burke, *Electrochem. Soc. Interface* **2008**, *17*, 38.

Manuscript received: January 7, 2019
Accepted manuscript online: January 23, 2019
Version of record online: February 20, 2019